The European Large Area *ISO* Survey — IV. The preliminary 90-m luminosity function

Journal Item

Mon. Not. R. Astron. Soc. **322**, 262–268 (2001)

The European Large Area *ISO* Survey – IV. The preliminary 90-μm luminosity function

S. Serjeant,[1★] A. Efstathiou,[1] S. Oliver,[1,2] C. Surace,[1] P. Héraudeau,[3]
M. J. D. Linden-Vørnle,[4] C. Gruppioni,[5] F. La Franca,[6] D. Rigopoulou,[7] T. Morel,[1]
H. Crockett,[1] T. Sumner,[1] M. Rowan-Robinson[1] and M. Graham[1]

[1]*Astrophysics Group, Blackett Laboratory, Imperial College, Prince Consort Road, London SW7 2BW*
[2]*Astronomy Centre, CPES, University of Sussex, Falmer, Brighton BN1 9QJ*
[3]*Max-Planck-Institut für Astronomie, Königstuhl 17, D69117, Heidelberg, Germany*
[4]*Danish Space Research Institute, 30 Juilane Maries Vej, DK-2100 Copenhagen ø, Denmark*
[5]*Osservatorio Astronomico di Bologna, via Ranzani 1, 40127 Bologna, Italy*
[6]*Dipartimento di Fisica E. Amaldi, Via della Visca Navale 84, Rome, Italy*
[7]*Max-Planck-Institut für extraterrestrische Physik Giessenbachstraße, 85748 Garching, Germany*

Accepted 2000 September 26. Received 2000 September 12; in original form 2000 July 10

ABSTRACT

We present the luminosity function of 90-μm-selected galaxies from the European Large Area *ISO* Survey (ELAIS), extending to $z = 0.3$. Their luminosities are in the range $10^9 < h_{65}^{-2} L/\mathrm{L}_\odot < 10^{12}$, i.e. non-ultraluminous. From our sample of 37 reliably detected galaxies in the ELAIS S1 region from the Efstathiou et al. $S_{90} \geqslant 100\,\mathrm{mJy}$ data base, we have found optical, 15-μm or 1.4-GHz identifications for 24 (65 per cent). We have obtained 2dF and UK Schmidt FLAIR spectroscopy of 89 per cent of identifications to rigid multivariate flux limits. We construct a luminosity function assuming that (i) our spectroscopic subset is an unbiased sparse sample, and (ii) there are no galaxies that would not be represented in our spectroscopic sample at *any* redshift. We argue that we can be confident of both assumptions. We find that the luminosity function is well described by the local 100-μm luminosity function of Rowan-Robinson, Helou & Walker. *Assuming* this local normalization, we derive luminosity evolution of $(1 + z)^{2.45 \pm 0.85}$ (95 per cent confidence). We argue that star formation dominates the bolometric luminosities of these galaxies, and we derive comoving star formation rates in broad agreement with the Flores et al. and Rowan-Robinson et al. mid-infrared-based estimates.

Key words: surveys – galaxies: evolution – galaxies: formation – galaxies: starburst – cosmology: observations – infrared: galaxies.

1 INTRODUCTION

The study of the star formation history of the Universe is an extremely active field, in which much of the current debate is centred on the uncertainties in dust obscuration. Selecting star-forming galaxies in the ultraviolet is relatively cheap in observing time, but such selection makes the samples extremely sensitive to dust obscuration. Detecting the reprocessed starlight requires sub-millimetre surveys (e.g. Smail, Ivison & Blain 1997; Hughes et al. 1998; Barger et al. 1998, 1999; Eales et al. 1999; Peacock et al. 2000; Ivison et al. 2000a,b; Dunne et al. 2000) and/or space-based mid–far-infrared surveys (e.g. Rowan-Robinson et al. 1997; Taniguchi et al. 1997; Kawara et al. 1998; Flores et al. 1999; Puget et al. 1999; Oliver et al. 2000; see e.g. Oliver 2001 for a review). As such, the European Large Area *ISO* Survey (ELAIS) is well-placed for the study of the evolution and obscuration of the star formation in the Universe, and strong constraints at $z \lesssim 1$ are possible from ELAIS (Oliver et al. 2000).

The scientific aims and strategy of ELAIS were presented in detail in Paper I (Oliver et al. 2000). In Papers II and III (Serjeant et al. 2000; Efstathiou et al. 2000) we presented respectively the ELAIS preliminary analysis source counts from the CAM (6.7 and 15 μm) and PHOT (90 μm) instruments on *ISO*. The 90-μm sample covered 11.6 square degrees, and the source counts were found to agree well at the bright end with the *IRAS* 100 μm counts. Excellent agreement was also achieved with a parallel independent pipeline (Surace et al., in preparation).

In this paper we present the first 90-μm luminosity function from our initial spectroscopic campaigns in the ELAIS S1 field (Gruppioni et al., in preparation; La Franca et al., in preparation;

★ E-mail: s.serjeant@ic.ac.uk

Linden-Vørnle et al., in preparation; Oliver et al., in preparation). Section 2 defines our sample. In Section 3 we use this catalogue to derive a 90-μm luminosity function. We discuss the implications of our results in Section 4. We assume $H_0 = 65\,\mathrm{km\,s^{-1}\,Mpc^{-1}}$, $\Omega_0 = 1$ and $\Lambda = 0$ throughout.

2 SAMPLE SELECTION AND DATA ACQUISITION

The parent sample for this study is the preliminary analysis catalogue of Paper III, with 90-μm fluxes satisfying $S_{90} > 100\,\mathrm{mJy}$. The completeness of this sample falls approaching this limit, but has been well-quantified with simulations (fig. 6 of Paper III). We will use the calibration adopted in Paper III. The 90-μm flux calibration is still uncertain to within ~30 per cent, as discussed in Paper III; however, in order to be consistent with the 100 μm *IRAS* source counts (assuming $S_{90} \simeq S_{100}$), the flux calibration has to be very close to the Paper III value. Therefore, when we compare our 90-μm luminosity function with the local 100-μm luminosity function below, we will treat the flux calibration as being accurately known. Nevertheless, in predicting the redshift distributions of other 90-μm surveys, we will not neglect the flux calibration systematics.

We restrict our study to the ELAIS S1 field with 90-μm, 1.4-GHz and 15-μm survey coverage, which covers 3.96 square degrees and has the most extensive available optical spectroscopy. Large-scale structure variations are negligible in the comoving volume of the total ELAIS survey, but the ELAIS S1 field has slightly lower source counts than the global average. Consequently we reduced the effective area by 20 per cent (a factor of 0.8) to make the S1 counts normalization match the whole survey, to account for any possible large-scale structure fluctuations. (This correction is smaller than the errors in the luminosity function derived below.) We sought identifications of this sample using (i) the Automatic Plate Measuring machine (APM), (ii) sub-mJy decimetric radio sources from our Australia Telescope Compact

Table 1. ELAIS S1 90-μm sample. The 90-μm photometry has a ~30 per cent possible systematic uncertainty (see Paper III), and the 15-μm photometry is subject to a possible systematic scaling to fainter fluxes by up to a factor of ~1.5 (see Paper II). We assume $H_0 = 65\,\mathrm{km\,s^{-1}\,Mpc^{-1}}$, $\Omega_0 = 1$ and $\Lambda = 0$, and bolometric luminosities are calculated at 90 μm assuming a constant νL_ν spectrum. The maximum accessible redshifts $z_{\max}$ quoted assume no evolution, and are labelled respectively as P, R, O and C for maximum redshifts imposed by the 90-μm PHOT flux limit, the radio flux limit, the optical magnitude limit and the CAM flux limit. Two galaxies (ELAISP90_J003721-434228 and ELAISP90_J003021-423657) are Seyfert 2 galaxies, and two further galaxies (ELAISP90_J003431-433806 and ELAISP90_J003133-425100) have an early-type spectrum; all the remainder show starburst emission-line spectra. Also listed are four redshifts for candidate optical identifications with the optical magnitudes listed, but which lack other multiwavelength detections and are too faint optically to be certain that the correct identification has been found. All four such identifications show starburst emission-line spectra, but nevertheless are excluded from the luminosity function analysis as they fail the strict selection function defined in the text.

Name	RA (J2000)	Dec. (J2000)	S_{90}/Jy	S_{15}/mJy	$S_{1.4}$/mJy	R	z	$z_{\max}$	$L/\mathrm{L}_\odot$
ELAISP90_J003857-424358	00 38 57.7	−42 43 58.8	0.43	2.9	0.964				
ELAISP90_J003056-441633	00 30 57.0	−44 16 33.6	0.35	4.9		13.7	0.019	0.0351^{P}	2.8×10^{9}
ELAISP90_J003510-435906	00 35 10.5	−43 59 6.0	0.41	9.6		12.1	0.136	0.272^{P}	1.7×10^{11}
ELAISP90_J003431-432613	00 34 31.6	−43 26 13.2	0.59			14.0	0.053	0.127^{P}	3.7×10^{10}
ELAISP90_J003914-430437	00 39 14.8	−43 04 37.2	1.79	16.2		11.6	0.012	0.049^{P}	5.7×10^{9}
ELAISP90_J003021-423657	00 30 21.1	−42 36 57.6	1.17	22.3		16.0	0.149	0.493^{P}	6.0×10^{11}
ELAISP90_J003459-425718	00 34 59.0	−42 57 18.0	0.55	5.5	1.371	14.9	0.055	0.101^{R}	3.7×10^{10}
ELAISP90_J003134-424420	00 31 34.5	−42 44 20.4	0.31			13.1	0.027	0.048^{P}	5.1×10^{9}
ELAISP90_J003242-423314	00 32 42.9	−42 33 14.4	0.24	2.6	0.463	15.2	0.053	0.081^{P}	1.5×10^{10}
ELAISP90_J003615-424344	00 36 15.4	−42 43 44.4	0.31			17.2	0.115		
ELAISP90_J003516-440448	00 35 16.1	−44 04 48.0	0.29						
ELAISP90_J003741-440227	00 37 41.6	−44 02 27.6	0.21			19.9	0.348		
ELAISP90_J003431-433806	00 34 31.2	−43 38 6.0	0.75		0.595	18.4	0.199	0.357^{O}	6.8×10^{11}
ELAISP90_J003405-423816	00 34 5.3	−42 38 16.8	0.23						
ELAISP90_J003358-441102	00 33 58.2	−44 11 2.4	0.23	5.0		18.9	0.305	0.446^{O}	5.2×10^{11}
ELAISP90_J003501-423852	00 35 1.9	−42 38 52.8	0.28		0.606	15.9	0.054	0.090^{P}	1.8×10^{10}
ELAISP90_J003254-424608	00 32 54.2	−42 46 8.4	0.46	2.5	0.469	17.7	0.190	0.207^{C}	3.8×10^{11}
ELAISP90_J003531-423314	00 35 31.4	−42 33 14.4	0.16						
ELAISP90_J003635-430148	00 36 35.7	−43 01 48.0	0.12	4.5	0.358	21.5			
ELAISP90_J003019-432006	00 30 19.8	−43 20 6.0	0.20						
ELAISP90_J003839-422324	00 38 40.0	−42 23 24.0	0.14						
ELAISP90_J003014-440509	00 30 14.3	−44 05 9.6	0.10	3.6					
ELAISP90_J003912-431203	00 39 12.2	−43 12 3.6	0.15	5.0		14.8			
ELAISP90_J003133-425100	00 31 33.9	−42 51 0.0	0.11	6.3		18.0	0.211	0.222^{P}	1.1×10^{11}
ELAISP90_J003304-425212	00 33 4.3	−42 52 12.0	0.19	1.4		15.6			
ELAISP90_J003046-432204	00 30 46.4	−43 22 4.8	0.11	6.2		15.6	0.073	0.075^{P}	1.3×10^{10}
ELAISP90_J003027-433050	00 30 27.7	−43 30 50.4	0.11	4.9		15.7	0.072	0.074^{P}	1.2×10^{10}
ELAISP90_J002845-424420	00 28 45.5	−42 44 20.4	0.11						
ELAISP90_J003719-421955	00 37 19.4	−42 19 55.2	0.16						
ELAISP90_J003725-424554	00 37 25.2	−42 45 54.0	0.12						
ELAISP90_J003731-440758	00 37 31.3	−44 07 58.8	0.32			20.0			
ELAISP90_J003625-441127	00 36 25.0	−44 11 27.6	0.14		4.265				
ELAISP90_J003721-434228	00 37 21.5	−43 42 28.8	0.12	17.3	0.451	17.4	0.225	0.248^{P}	1.4×10^{11}
ELAISP90_J003348-433032	00 33 48.3	−43 30 32.4	0.15						
ELAISP90_J003149-423628	00 31 49.2	−42 36 28.8	0.11						
ELAISP90_J003244-424803	00 32 44.4	−42 48 3.6	0.12	1.2		19.0	0.192		
ELAISP90_J003323-432634	00 33 23.2	−43 26 34.8	0.19			18.7	0.316		

Array (ATCA) imaging (Gruppioni et al. 1999), and (iii) our ELAIS ISOCAM 6.7- and 15-μm catalogues (Paper II). By randomizing our 37 catalogue positions in the cross-correlation, we found that <1 optical APM identification brighter than $R = 17$ should occur by chance within the error ellipses of all our PHOT sources, and similarly restricted the association radius for the CAM and radio catalogues. Optical spectroscopy was obtained at the 2° field (2dF) at the Anglo-Australian Telescope (AAT), with the Fibre Linked Array Image Reformatter (FLAIR) spectrograph at the UK Schmidt and with the Danish Faint Object Spectrograph and Camera (DFOSC) at the Danish 1.54-m telescope at the European Southern Observatory. The optical spectroscopic catalogue will appear in future papers in this series. Of the 37 reliably detected galaxies, 24 had multiwavelength identifications, of which 18 are above the combined multivariate flux limits discussed above. Of these, we have obtained optical spectroscopy of 89 per cent. The ELAIS S1 90-μm sample is presented in Table 1 with the cross-identifications and available redshifts. This table also lists redshifts for four identifications for which the identification is uncertain. These galaxies fail the strict selection function defined below and are excluded from the luminosity function analysis. Two galaxies (ELAISP90_J003721-434228 and ELAISP90_J003021-423657) are Seyfert 2 galaxies, and two further galaxies (ELAISP90_J003431-433806 and ELAISP90_J003133-425100) have an early-type spectrum; all the remainder (including the four excluded identifications) show starburst emission-line spectra.

3 RESULTS: THE 90-μM LUMINOSITY FUNCTION

Our selection function is as follows. In order to be in the spectroscopic target list, a 90-μm galaxy must have either (i) a reliable optical identification brighter than $R = 17$, or (ii) a reliable 15-μm or 1.4-GHz identification, together with an optical identification brighter than $R = 20$. The 15-μm identifications were made to $S_{15} \geqslant 2\,\mathrm{mJy}$, and the radio identifications to 0.2–0.4 mJy depending on position (Gruppioni et al. 1999). Only 90-μm galaxies in the area with radio and 15-μm survey coverage were considered. We used the M82 starburst model from Rowan-Robinson et al. (1997) to estimate the K-corrections, with $S_{60\,\mu\mathrm{m}} = 120 S_{1.4\,\mathrm{GHz}}$ and a radio spectral index of $\mathrm{d}\log_{10} S/\mathrm{d}\log_{10}\nu = -0.8$. For optical K-corrections we assumed an optical spectral index of -3. The redshift–luminosity plane is shown in Fig. 1, with bolometric luminosities calculated at 90 μm assuming constant νL_ν (for ease of conversion to other luminosity scales). Our method for calculating the luminosity function in the face of this complicated selection function is dealt with in the appendix. Note that our method relies on the underlying assumption that no galaxies are missing at *all* redshifts owing to the multivariate flux limits. However, we can be confident of this in our case, as any sufficiently low-redshift galaxy will have an optical identification that will pass criterion (i) of our selection function. A hypothetical local population of very optically faint but far-infrared-bright galaxies can already be excluded from *IRAS* samples. We must also assume that our 89 per cent complete optical spectroscopy is a random sparse sample of the total identifications (although not necessarily of the total 90-μm sample). Although with our current spectroscopic sample this is an a posteriori selection rather than an a priori one, there were no selection biases in the spectroscopic data acquisition that could skew the sample selection function. We

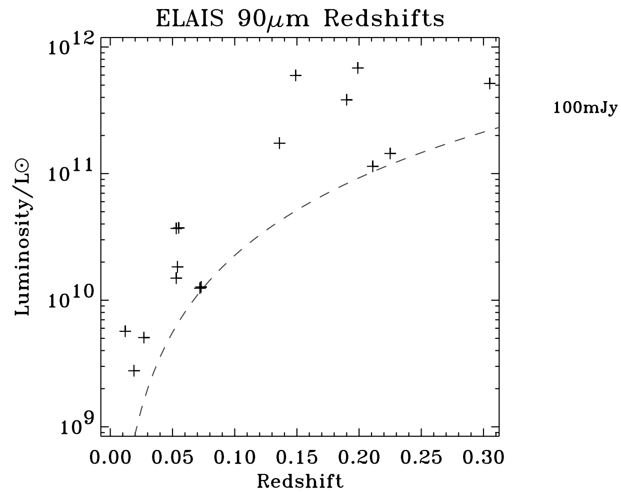

Figure 1. Redshift–luminosity plane. The 100-mJy flux limit is marked.

therefore corrected our effective areal coverage by a factor of 0.89 to account for the small optical spectroscopic incompleteness.

The integral luminosity function is given by

$$\Phi(>L) = \sum_{L_i > L} V_{\max,i}^{-1}, \tag{1}$$

where the sum is performed over all objects having luminosities greater than L. In Fig. 2 we show this integral luminosity function, and compare it with the local 100-μm luminosity function derived by Rowan-Robinson, Helou & Walker (1987) (binned data). The latter was derived from a sample in the North Galactic Pole, and is subject to possible large-scale structure variations. To estimate this, we compared the normalization of their 60-μm luminosity function with that of Saunders et al. (1990), and derived a correction factor of 0.77 to the normalization of their 100-μm luminosity function. The best-fitting function to these local data is plotted as a full line. The adopted functional form is identical to that of Saunders et al. (1990):

$$\phi(L) = \phi_* \left(\frac{L}{L_*}\right)^{1-\alpha} \exp\left[-\frac{1}{2\sigma^2}\log^2\left(1+\frac{L}{L_*}\right)\right], \tag{2}$$

and the best-fitting parameters are given in Table 2. Also plotted in this figure are the models of Rowan-Robinson (2000).

The hatched area shows the $\pm 1\sigma$ errors from our sample. There is a marginally significant excess at the highest luminosities. The $\langle V/V_{\max}\rangle$ statistic for this sample is 0.54 ± 0.07; a Kolmogorov–Smirnov test on the $V/V_{\max}$ distribution shows only a 34 per cent probability of inconsistency with the top-hat distribution $U[0,1]$. Assuming $(1+z)^3$ luminosity evolution (Fig. 2) gives $\langle V/V_{\max}\rangle = 0.51 \pm 0.07$, and, in both the evolving and non-evolving models, a Kolmogorov–Smirnov test on the observed luminosity distribution also gives acceptable confidence levels. Our spectroscopic subsample on its own is therefore not sufficiently large to detect evolution reliably.

A much stronger constraint on the strength of the evolution comes from the source counts slope. The 90-μm counts in the entire ELAIS areas are significantly non-Euclidean (Paper III), but the counts do show a suprising upturn at the faintest end (Fig. 3). The cause of this upturn is not clear, but it is too large to be entirely attributable to uncertainties in the completeness correction. One possibility is that some of the faintest sources are spurious glitch events, but all the sources have been eyeballed and

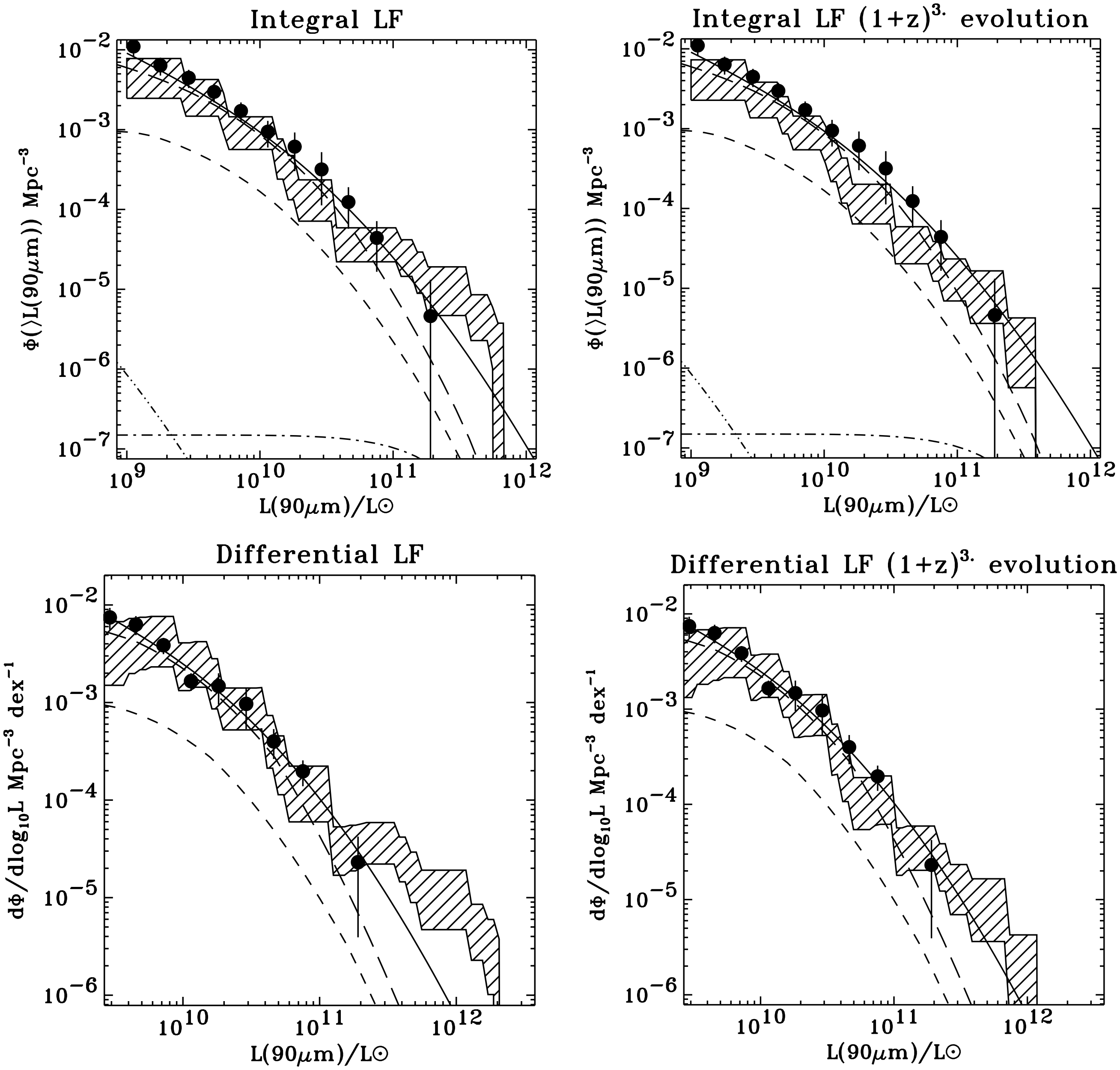

Figure 2. Luminosity function assuming no evolution (left) and $(1+z)^3$ luminosity evolution (right). The upper panels show the integral luminosity function; the lower panels show the differential form. The hatched area is the $\pm 1\sigma$ error region from this study. For the differential counts the hatched area indicates the error on the luminosity function in a ±0.5-dex bin; the differential counts are therefore effectively smoothed by a 1-dex boxcar. The data points show the local 100-μm luminosity function of Rowan-Robinson et al. (1987), and the full line is a fit to these local data. The broken lines show the populations in the Rowan-Robinson (2000) model. The long-dashed line denotes the 'cirrus-like' population, i.e. galaxies with bolometric luminosities dominated by new stars heating previously created dust. Note that this population is not necessarily identified with NGC 6090-like cirrus galaxies. The short-dashed line denotes the starburst population; the dash–dotted indicates Arp 220-like galaxies; the dash–double-dotted line shows the AGN population.

accepted by at least two observers. Such a glitch population would have to be somewhat pathological. Evidence for comparably strong evolution at <200 mJy in the Lockman Hole is also reported by Matsuhara et al. (2000) based on model fits to the fluctuations in their 90-μm maps, consistent with the faintest ELAIS points. Nevertheless, in the absence of a clear model-independent interpretation, we confine our source count fits to the >200 mJy region. We note that the sources used in the luminosity function are all reliably cross-identified at other wavelengths. The source counts at >200 mJy are in good agreement with the Lockman Hole counts from Linden-Vørnle et al. (2000) (Fig. 3), who use a very different source extraction and flux calibration procedure from ELAIS. The ELAIS and Lockman counts for the faintest bin in Fig. 3 (165–294 mJy) are 27 ± 4 and $22 \pm 9\,\mathrm{deg}^{-2}\,\mathrm{dex}^{-1}$ respectively, and in the brightest bin (294–522 mJy) are 19 ± 4 and $4^{+9}_{-3.3}\,\mathrm{deg}^{-2}\,\mathrm{dex}^{-1}$ respectively. Note that this represents only a single source in the Lockman Hole, so Poissonian errors would underestimate the error in this case. The $\pm 1\sigma$ bounds in the case of one observed source are 0.18–3.3, and all the remaining errors quoted in the counts are $\pm 1\sigma$ Poissonian errors.

If we *assume* that the local luminosity function derived above

Table 2. Best-fitting parameters of the local luminosity function, with $\sigma = 0.724$ assumed. The reduced χ^2 of the best fit is 0.66.

$\phi^* h_{65}^{-3}$	$\log_{10} L^* h_{65}^{2}/\mathrm{L}_{\odot}$	α
5.4 ± 1.8	9.67 ± 1.47	1.73 ± 0.04

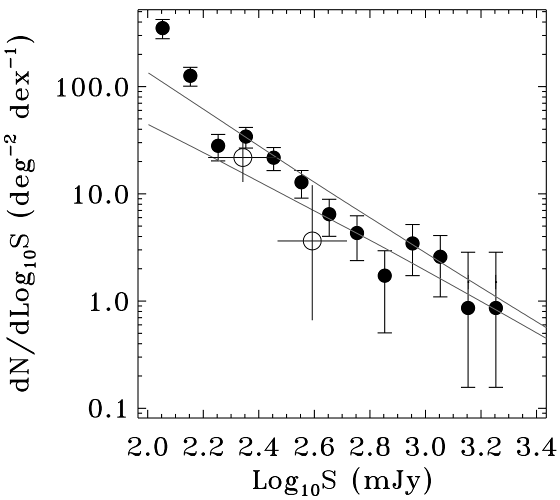

Figure 3. ELAIS source counts at 90 μm, compared with a no-evolution model (shallow curve) and the $(1+z)^3$ luminosity evolution model (steeper curve). The no-evolution curve has a slightly shallower slope than its Euclidean equivalent. Also shown as open symbols are the Lockman Hole counts from Linden-Vørnle et al. (2000). All errors are Poissonian, except in the case of a single object in a bin for which the $\pm 1\sigma$ bounds on the number of objects in the bin are 0.18–3.3.

undergoes $(1+z)^\alpha$ luminosity evolution, we can obtain a constraint on the evolution parameter α. Note that this is relatively insensitive to the flux calibration uncertainty (Paper III). The correct relative normalization between 90 and 100 μm for these purposes is one that achieves continuity in the source counts. The current 90-μm calibration satisfies this almost exactly (Paper III) in that the bright end of the 90-μm PHOT counts dovetails with the faint end of the 100-μm *IRAS* counts, with little room for error in the *relative* calibration. The Kolmogorov–Smirnov test on the shape of the source counts yields a lower limit of $\alpha > 1.5$ at 95 per cent confidence, and no-evolution models can be excluded at the 98 per cent level. Stronger constraints still are possible if we include the normalization of the source counts. Our goodness-of-fit statistic for this is $P_{\mathrm{KS}} \times P_{\tilde{\mathrm{N}}}$, where P_{KS} is the significance level of rejecting the model of the shape of the source counts, and $P_{\tilde{\mathrm{N}}}$ is the significance level of rejecting the predicted normalization. The distribution function for such statistics is quoted in e.g. Dunlop & Peacock (1990). We obtain $\alpha = 2.45 \pm 0.85$ (95 per cent confidence). This is stronger than the constraint obtained purely from a $V/V_{\max}$ analysis of the spectroscopic sub-sample, partly because the number of galaxies comprising the source counts is much larger, partly also because we have assumed a fixed functional form for the zero-redshift luminosity function, but mainly because we have set the $z = 0$ normalization from *IRAS*.

4 DISCUSSION AND CONCLUSIONS

We have found that both the shape and the normalization of the 90-μm luminosity function are well-described by the local luminosity function of Rowan-Robinson et al. (1987), with evolution consistent with $(1+z)^{2.45\pm0.85}$ pure luminosity evolution, using the transformation $S_{100} \simeq S_{90}$. Pure density evolution is already excluded in this population as it conflicts with sub-mJy radio source counts (Rowan-Robinson et al. 1993).

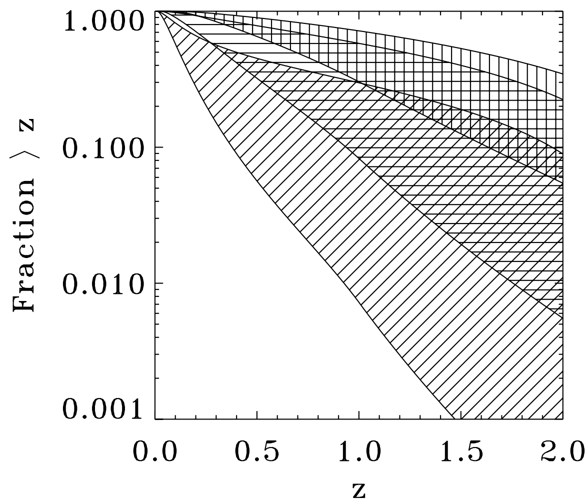

Figure 4. Predicted cumulative redshift distribution for surveys at 100κ mJy (diagonal hatching), 10κ mJy (horizontal hatching) and 1κ mJy (vertical hatching), where $\kappa = 1 \pm 0.3$ indicates the uncertainty in the ELAIS PHOT absolute flux calibration. The bounds of the hatched areas are dominated by the assumed maximum redshift at which luminosity evolution occurs.

We can use these results to predict the redshift ranges of current and future 90-μm surveys. We assume that the evolution extends to between $z = 1$ and 2 and is then non-evolving. Fig. 4 shows the 95 per cent confidence limit for surveys of various depths, incorporating the uncertainty in the ELAIS 90-μm absolute flux calibration. One corollary is that at least 10 per cent of the currently unidentified 90-μm galaxies in ELAIS extend to $z > 0.5$, possibly even $z > 2$.

Is it reasonable to assume that star formation dominates the bolometric luminosities of our 90-μm sample? Genzel et al. (1998), Lutz et al. (1998) and Rigopoulou et al. (1999) have presented mid-infrared spectroscopy of ultraluminous galaxies ($L \geqslant 10^{12}\,\mathrm{L}_{\odot}$) in the same redshift interval as our sample, and using the polycyclic aromatic hydrocarbon (PAH) features as a star formation indicator find that star formation dominates the bolometric power outputs in 70–80 per cent of ultraluminous infrared galaxies (ULIRGs). The active galactic nucleus (AGN) bolometric fraction derived in this way decreases monotonically at lower luminosities (e.g. Lutz et al. 1998). In local infrared galaxies between 10^{11} and $10^{12}\,\mathrm{L}_{\odot}$, ~15 per cent have Seyfert 2 spectra (Telesco 1988), although care should be taken in interpreting AGN dominance from optical spectra (e.g. Lutz, Veilleux & Genzel 1999; Taniguchi et al. 1999). At $L < 10^{11}\,\mathrm{L}_{\odot}$ most local infrared galaxies are single, gas-rich spirals (e.g. Sanders & Mirabel 1996) in which many lines of argument point to starburst dominance in the infrared (e.g. Telesco 1988): for example, the similarity of the spectral energy distributions to those of Galactic star-forming regions; the linear L_{IR}–L_{CO} correlation over many orders of magnitude in luminosity; and optical/infrared spectroscopic confirmation of star formation activity. It therefore seems likely that our sub-ultraluminous population should not be powered by active nuclei, as is also suggested by the low fraction of spectra in our sample (10 per cent) with Seyfert 2 features. (This does not imply that AGN activity cannot be present at a weak or bolometrically negligible level: e.g. Ho, Filippenko & Sargent 1997.) At the lowest luminosities there may be a significant contribution from cirrus which is at least partly illuminated by the old stellar population in the galaxies (Telesco 1988; Morel et al. 2001), although such galaxies nevertheless also still obey the starburst radio–far-infrared relation (e.g. Condon 1992). We conclude that the galaxies in our sample have their bolometric luminosities dominated by star formation.

The Saunders et al. (1990) local luminosity density implies a local star formation rate of $0.023 \pm 0.002\,\mathrm{M}_{\odot}\,\mathrm{yr}^{-1}\,\mathrm{Mpc}^{-3}$ (Oliver, Gruppioni & Serjeant 2001) assuming a Salpeter initial mass function from 0.1 to $125\,\mathrm{M}_{\odot}$. Our results imply that this rises to $0.036 \pm 0.009\,\mathrm{M}_{\odot}\,\mathrm{yr}^{-1}\,\mathrm{Mpc}^{-3}$ by $z = 0.2$ (95 per cent confidence), significantly higher than the Tresse & Maddox (1998) Hα-based estimate of $0.022 \pm 0.007\,\mathrm{M}_{\odot}\,\mathrm{yr}^{-1}\,\mathrm{Mpc}^{-3}$. (Note that the two Seyfert 2 spectra in our sample are at the brightest end of the luminosity function where the contribution to the luminosity density is the smallest. The luminosity density is dominated by the galaxies around or below the break in Table 2.) We believe that this is due to two factors: first, the Hα-based estimates are not immune to extinction effects, even if Balmer decrement reddening corrections are performed (e.g. Serjeant, Gruppioni & Oliver 2001); secondly, the Tresse & Maddox (1998) survey area is sufficiently small to be affected by large-scale structure (e.g. Oliver et al. 2001). ELAIS is immune to these problems, as the cosmic variance over the PHOT survey area is <20 per cent at $z < 0.3$ (Paper I). These star formation rates are, however, consistent with extrapolations from those derived from mid-infrared data at higher redshift by Flores et al. (1999) and Rowan-Robinson et al. (1997).

The prospects for improving on the results presented here are excellent. A large-scale spectroscopic follow-up of the ELAIS northern areas is currently underway, which will have a major impact on the science analysis of ELAIS. In particular, the ELAIS 15-μm luminosity function will probe higher redshifts than accessible to PHOT at 90 μm, from which the 15-μm luminosity density can constrain the cosmic star formation history (e.g. Serjeant, in preparation).

ACKNOWLEDGMENTS

We thank Dave Clements and the anonymous referee for helpful comments on this paper. This work was supported by PPARC (grant number GR/K98728) and by the EC TMR Network programme (FMRX-CT96-0068).

REFERENCES

Barger A. J., Cowie L. L., Sanders D. B., Fulton E., Taniguchi Y., Sato Y., Kawara K., Okuda H., 1998, Nat, 394, 248
Barger A., Cowie L. L., Smail I., Ivison R. J., Blain A. W., Kneib J.-P., 1999, AJ, 117, 2656
Condon J. J., 1992, ARA&A, 30, 575
Dunlop J. S., Peacock J. D., 1990, MNRAS, 247, 19
Dunne L., Eales S., Edmunds M., Ivison R., Alexander P., Clements D. L., 2000, MNRAS, 315, 115
Eales S., Lilly S., Gear W., Dunne L., Bond J. R., Hammer F., Le Févre O., Crampton D., 1999, ApJ, 515, 518
Efstathiou A. et al., 2000, MNRAS, 319, 1169 (Paper III)
Flores H. et al., 1999, ApJ, 517, 148
Genzel R. et al., 1998, ApJ, 498, 579
Gruppioni C. et al., 1999, MNRAS, 305, 297
Ho L. C., Filippenko A. V., Sargent W. L. W., 1997, ApJS, 112, 315
Hughes D. et al., 1998, Nat, 394, 421
Ivison R. J., Dunlop J. S., Smail I., Dey A., Liu M. C., Graham J. R., 2000a, ApJ, 542, 27
Ivison R. J., Smail I., Barger A. J., Kneib J.-P., Blain A. W., Owen F. N., Kerr T. H., Cowie L. L., 2000b, MNRAS, 315, 209
Kawara K. et al., 1998, A&A, 336, L9
Linden-Vørnle M. J. D. et al., 2000, A&A, 359, 51
Lutz D., Spoon H. W. W., Rigopoulou D., Moorwood A. F. M., Genzel R., 1998, ApJ, 505, L103
Lutz D., Veilleux S., Genzel R., 1999, ApJ, 517, L13
Matsuhara H. et al., 2000, A&A, 361, 407
Morel T. et al., 2001, MNRAS, submitted
Oliver S., 2001, in Matsumoto T., Shibai H., eds, Mid- and Far-Infrared Astronomy and Future Space Missions, ISAS Report Special Edition (SP No. 14), in press
Oliver S. et al., 2000, MNRAS, 316, 749(Paper I)
Oliver S., Gruppioni C., Serjeant S., 2001, MNRAS, submitted (astro-ph/9808260)
Peacock J. et al., 2000, MNRAS, 318, 535
Puget J. L., 1999, A&A, 345, 29
Rigopoulou D., Spoon H. W. W., Genzel R., Lutz D., Moorwood A. F. M., Tran Q. D., 1999, AJ, 118, 2625
Rowan-Robinson M., 2000, ApJ, submitted
Rowan-Robinson M., Helou G., Walker D., 1987, MNRAS, 227, 589
Rowan-Robinson M., Benn C. R., Lawrence A., McMahon R. G., Broadhurst T. J., 1993, MNRAS, 263, 123
Rowan-Robinson M. et al., 1997, MNRAS, 289, 490
Sanders D. B., Mirabel I. F., 1996, ARA&A, 34, 749
Saunders W., Rowan-Robinson M., Lawrence A., Efstathiou G., Kaiser N., Ellis R. S., Frenk C. S., 1990, MNRAS, 242, 318
Serjeant S., Gruppioni C., Oliver S., 2001, MNRAS, submitted (astro-ph/9808259)
Serjeant S. et al., 2000, MNRAS, 316, 768 (Paper II)
Smail I., Ivison R. J., Blain A. W., 1997, ApJ, 490, L5
Taniguchi Y. et al., 1997, A&A, 328, L9
Taniguchi Y., Yoshino A., Ohyama Y., Nishiura S., 1999, ApJ, 514, 660
Telesco C. M., 1988, ARA&A, 26, 343
Tresse L., Maddox S. J., 1998, ApJ, 495, 691

APPENDIX A: $1/V_{\mathrm{MAX}}$ WITH MULTIVARIATE FLUX LIMITS

In a volume-limited non-evolving sample, the comoving number density of objects can be calculated trivially:

$$\phi = \frac{N}{V} = \frac{1}{V}\sum_{i=1}^{N} 1, \tag{A1}$$

where V is the volume and N the number of objects. Suppose that the sample is incomplete in whatever way, and that the probability of the ith object being contained in the sample is p_i. Provided that none of the p_is in the underlying galaxy population is zero, the comoving number density in an observed sample of N_{obs} objects can be expressed as

$$\phi = \frac{1}{V}\sum_{i=1}^{N_{\mathrm{obs}}} p_i^{-1}. \tag{A2}$$

This will be an unbiased estimator of the underlying value.

Applying this formalism to our current data set, the incompleteness is due to the multivariate flux limits. We treat the (non-evolving) galaxies as sampling random redshifts within the volume, so that each p_i is the probability that such a galaxy would lie above the flux limits. The statement that the underlying p_is are all non-zero is equivalent to assuming that there are no galaxies (in the 90-μm luminosity range being considered) that would lie outside the selection criteria at all redshifts. We can be confident that this is the case, because any sufficiently local galaxy will have an optical identification passing criterion (i) of our selection function. A hypothetical population of far-infrared-luminous, optically faint galaxies can already be excluded from *IRAS*.

There are two equivalent ways of calculating the p_is. If we embed our flux-limited sample in a larger volume of size V_0, we can use the assumption that the population is non-evolving and the fact that the flux limits are monotonic in z to express the p_is as

$$p_i = \frac{V_{\max,i}}{V_0}, \tag{A3}$$

where $V_{\max,i}$ is the volume enclosed by the maximum redshift $z_{\max,i}$ at which the ith object is visible. Note that this is the smallest redshift at which the object fails *any* of the selection criteria. The number density in a sample of $N_{\rm obs}$ galaxies is then

$$\phi = \frac{1}{V_0}\sum_{i=1}^{N_{\rm obs}}\frac{V_0}{V_{\max,i}} = \sum_{i=1}^{N_{\rm obs}}\frac{1}{V_{\max,i}}. \tag{A4}$$

The rms error is simply

$$\Delta\phi = \sqrt{\sum_{i=1}^{N_{\rm obs}}\frac{1}{V^2_{\max,i}}}. \tag{A5}$$

An alternative but equivalent method of calculating the p_is is to model the incompleteness arising from some or all of the multivariate flux limits by introducing a weighting factor to the differential volume elements:

$$\mathrm{d}V' = \gamma(z, \ldots)\,\mathrm{d}V. \tag{A6}$$

The $z_{\max,i}$ values would then be calculated using the remaining unmodelled flux limits only. If all the flux limits have been modelled, then $\forall i\ z_{\max,i} = z_0$ where $V(z_0) = V_0$. The γ factor would drop to zero at some redshift if (under the previous method for calculating the $z_{\max,i}$) $z_0 > \max(z_{\max,i})$.

Here, our approach is to use the first method (equation A4) to treat the multivariate flux limits, as it is less model-dependent. However, we use a weighting function on the volume elements to correct for the ELAIS 90-μm completeness function (fig. 6 of Paper III):

$$V'_{\max,i} = \int_0^{z_{\max,i}} \gamma(z, S_i)\frac{\mathrm{d}V}{\mathrm{d}z}\mathrm{d}z, \tag{A7}$$

where S_i is the 90-μm flux of the ith object.

To calculate the luminosity function in a redshift bin, an additional top-hat selection function is applied in redshift space and incorporated into the calculation of the $z_{\max,i}$. The volume enclosed by the minimum redshift of the bin must also be subtracted from the $V_{\max,i}$ in equation (A3). We are currently confident that none of the underlying p_is is zero, but if we calculated the luminosity function in a series of redshift bins this would not necessarily be the case for all bins. For example, there are galaxies in Table 1 that only pass criterion (i) at the lowest redshifts, and these may be unobservable in principle in higher redshift bins. We would then need to make some model of the multivariate correlations to correct for the missing $p_i = 0$ galaxies. We therefore restrict ourselves to a single redshift range (de-evolving the galaxies if necessary), partly to avoid the model dependence of correcting for missing populations, but partly also because of our small sample size.

This paper has been typeset from a TEX/LATEX file prepared by the author.